Adsorption Mechanism of Supercritical Hydrogen in Internal and Interstitial Nanospaces of Single-Wall Carbon Nanohorn Assembly

K. Murata,[†] K. Kaneko,*[,‡] H. Kanoh,[‡] D. Kasuya,[§] K. Takahashi,[||] F. Kokai,[||] M. Yudasaka,[†] and S. Iijima[†,§,⊥]

Japan Science and Technology Corporation, c/o NEC Corporation, 34 Miyukigaoka, Tsukuba 305-8501, Japan, Physical Chemistry, Materials Science, Graduate School of Natural Science and Technology, and Center for Frontier Electronics and Photonics, Chiba University, 1-33 Yayoi, Inage, Chiba 263-8522, Japan, Department of Material Science and Engineering, Faculty of Science and Technology, Meijo University, 1501 Shiogamaguchi, Tenpaku, Nagoya 468-8502, Japan, Laser Research Center, Institute of Research and Innovation, 1201 Takada, Kashiwa, Chiba 277-0861, Japan, and NEC Corporation, 34 Miyukigaoka, Tsukuba 305-8501, Japan

Received: March 1, 2002; In Final Form: July 5, 2002

The exact physical adsorption amounts of supercritical hydrogen on the single-wall carbon nanohorn (SWNH) assemblies were determined at 77, 196, and 303 K. There are two physical adsorption sites of interstitial and internal spaces on SWNH assemblies. The interaction potential depths of interstitial and internal spaces are −1000 and −600 K, respectively. However, both hydrogen densities in interstitial and internal spaces were about 70 g L^{-1} at 77 K at 5 MPa, though the hydrogen densities in interstitial and internal spaces were 15 and 10 g L^{-1} at 303 K and 6.5 MPa. The similar enhancement in the internal spaces was observed even at 196 K. The additional stabilization by the strong fluid−fluid interaction due to the cluster formation in the internal spaces. On the other hand, hydrogen molecules adsorbed in the interstitial spaces cannot form the stable cluster owing to the space limitation. The enthalpy of adsorption supports the presence of the stable cluster of hydrogen adsorbed in the internal spaces below 303 K.

Introduction

Solid adsorbents that enable storage of fuel gases such as hydrogen and methane at high density have been requested for preservation of global environments, because hydrogen and methane vehicles can achieve low emissions of CO_2. However, it is difficult to store these gases in a highly dense state, because supercritical gases do not condense to liquid at room temperature even under high pressure.

Recent reports that carbon materials such as graphite nanofibers (GNF),[1] single wall carbon nanotubes (SWNT),[2,3] and modified carbon nanotubes[4] are hopeful for hydrogen storage have stimulated scientific activities on these materials. However, these experimental results are not well reproducible and many serious problems on the experiment are noted.[5,6] Also, grand-canonical Monte Carlo (GCMC) simulation studies[7,8] recommend further careful experimental studies.

One of the main reasons for the negative discussion of the experimental results is confusion in the gas storage concept. The gas storage includes four different concepts, namely, physical adsorption, chemisorption, absorption, and occlusion. Here physical adsorption and chemisorption are surface phenomena. In absorption and occlusion, the material taken up is distributed throughout the body of the absorbent. Molecules are dissociated into atoms, and the solid changes the structure to accept the atoms on occlusion. On the other hand, the solid structure varies on absorption of molecules without the molecular structure change in the case of absorption. These different concepts must be taken into account on evaluating the storage capacity. Physical adsorption is the most suitable mechanism to the application of fuel cells because it is reversible and both adsorption and desorption rates are very large, although the ordinary storage capacity by physical adsorption is limited because of weak hydrogen−hydrogen and hydrogen−carbon interactions. Although chemisorption is expected to realize the high adsorption capacity,[9] it is not reversible and desorption is impossible near ambient temperature. Then the effective capacity of chemisorption is not great. In addition, chemisorption for storage needs a long equilibrium time. On the other hand, absorption and occlusion are usually difficult in carbon materials because the carbon structure is rigid. However, if the adsorption process can occur, the hydrogen storage capacity should be large and it is reasonable.[10]

In this article, we show the physical adsorption of hydrogen on the single-wall carbon nanohorn (SWNH) by the gravimetric experiments, which is the most reliable measurement method for determination of the adsorbed quantity of supercritical gas. Although almost all single-wall carbon nanotubes (SWNTs) are low purity and contain catalyst metal, single-wall carbon nanohorns (SWNHs), being a new material of SWNT family, are very pure and the mass production is possible.[11] Thus, hydrogen adsorption on SWNH aggregates can be studied without any influence by catalyst metals and soots.

Experimental Section

The SWNH was prepared by the CO_2 laser ablation under Ar 101.32 kPa at room temperature without catalysts. The chemical purity is more than 98% and only oxygen can be

[†] Japan Science and Technology Corp.
[‡] Chiba University.
[§] Meijo University.
[||] Institute of Research and Innovation.
[⊥] NEC Corp.

10.1021/jp020583u CCC: $22.00
Published on Web 10/03/2002

TABLE 1: Microporosities and Particle Densities

sample	specific surface area, $m^2\ g^{-1}$	pore volume, $mL\ g^{-1}$	particle density, $g\ L^{-1}$
SWNH	308	0.11	1.25
SWNH-ox	1006	0.47	2.05

included due to exposure to the atmosphere.[12] Even the content of SWNH in percent in the sample is more than 95%.[11] As grown SWNH and SWNH oxidized at 693 K in O_2 for 10 min (SWNH-ox) were used as adsorbents.

The micropore structure of SWNH samples was determined by high-resolution N_2 adsorption at 77 K with the aid of the subtracting-pore-effect (SPE) method.[13,14] The particle density ρ_p[15] was determined by the high-pressure-helium buoyancy method.[16,17] The microporosity and particle density are shown in Table 1, which are the same as published before.[16,18,19] The microporosity of SWNH is much smaller than that of SWNH-ox. The small particle density of SWNH indicates the close hollow structure.[16] The great microporosity and particle density of SWNH-ox stem from the donation of "nanowindows" on the wall by the oxidation treatment, where the nanowindow is the hole that is opened on the SWNH wall. Consequently, the internal SWNH nanospaces of SWNH-ox are available for gas adsorption though the nanowindows.

The high-pressure hydrogen adsorption isotherm was measured at 77, 196, and 303 K by use of a Cahn microbalance (sensitivity 0.1 μg).[17] The high-purity hydrogen gas (99.99999%, Nippon Sanso) was used after purification with a liquid nitrogen trap. The pretreatment prior to the adsorption measurement was performed at a pressure less than 1 mPa and a temperature at 423 K for 2 h.

The buoyancy effect was corrected with the following equation.[6,20]

$$n_{ex} = n_{me} + \rho_{bulk} V_s \tag{1}$$

where n_{ex} is the surface excess mass (mg/g),[21−24] n_{me} is the measured weight per unit sample weight, ρ_{bulk} is the density of bulk gas, and V_s is the volume of the solid part and closed pores of the adsorbent (mL/g). Thus, n_{ex} can be experimentally determined, which is directly associated with the gas storage capacity.[25] However, the mean density of the adsorbed layer $\langle\rho_{ad}\rangle$ is convenient for thermodynamic analysis compared with surface excess mass.[24,26] Then the surface excess mass is transformed into $\langle\rho_{ad}\rangle$, as given by

$$\langle\rho_{ad}\rangle = \frac{n_{ex}}{V_{ad}} + \rho_{bulk} \tag{2}$$

where V_{ad} is the volume of adsorbed layer (mL/g). In this article, we assume V_{ad} as the micropore volume.[22,23,27,28]

Results and Discussion

Interaction Potential Structure. The TEM image of SWNHs is shown in Figure 1a. SWNHs form Dahlia flower like aggregates. A SWNH is illustrated in Figure 1b. The SWNH has both cone and tube parts that are basically composed of a graphene sheet. Physical adsorption of N_2 vapor on SWNH assemblies at 77 K can be understood using three sites that are distinguished by the interaction potential. Physical adsorption of hydrogen on SWNH assemblies is associated with the interaction potential structure. The interaction potential U_{sf} between SWNHs and a hydrogen molecule was calculated by the Steele-Bojan potential[19,29] for the triangular arrangement of

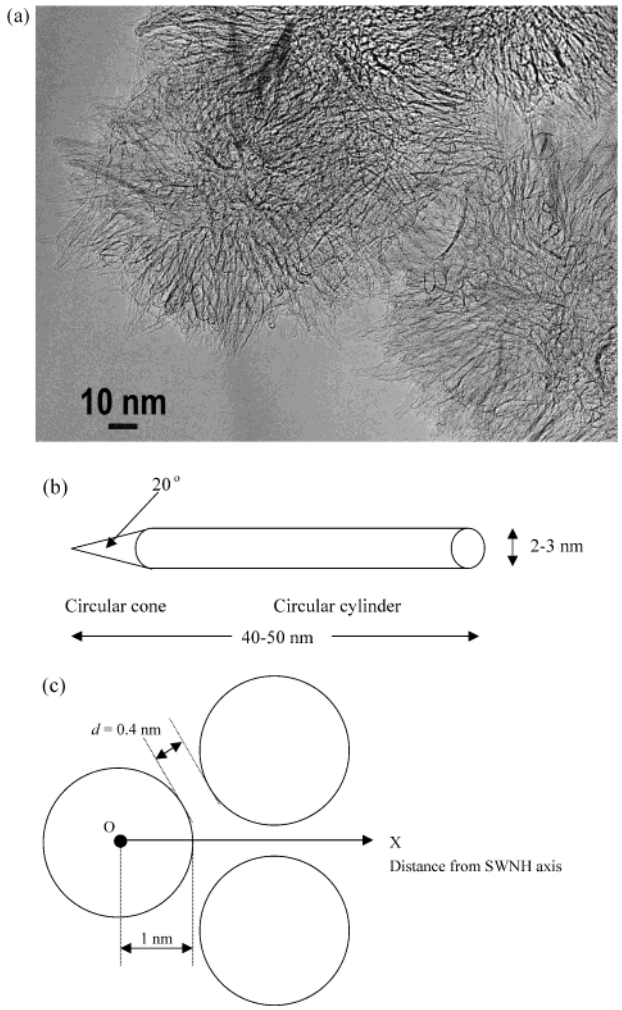

Figure 1. (a) TEM image of dahlia-flower like SWNH aggregates. (b) Illustration of a SWNH. (c) Unit assembly of SWNHs. Here the length of the cylinder part is shortened to express the whole particle geometry.

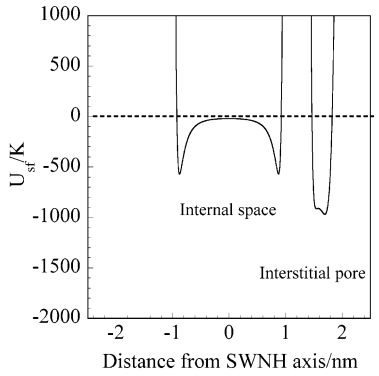

Figure 2. Interaction potential of a hydrogen molecule with SWNH along an O−X axis in Figure 1c.

parallel SWNH particles that are mutually distant by 2.8 nm of the inter-SWNH center.[30] Figure 2 shows the potential profile along the O−X direction in Figure 1c; here the origin is on the point O. The interaction potential of the interstitial site is the deepest (−1000 K). Here 1.2 nm of the radius of the tube was used. Although SWNH has a cone part that has a stronger interaction potential for the internal space, the pore volume due to the cone parts is not predominant (the volume percent is 7%) and we neglect the interaction potential in the cone part. As the interaction potential depth is not necessarily enough to

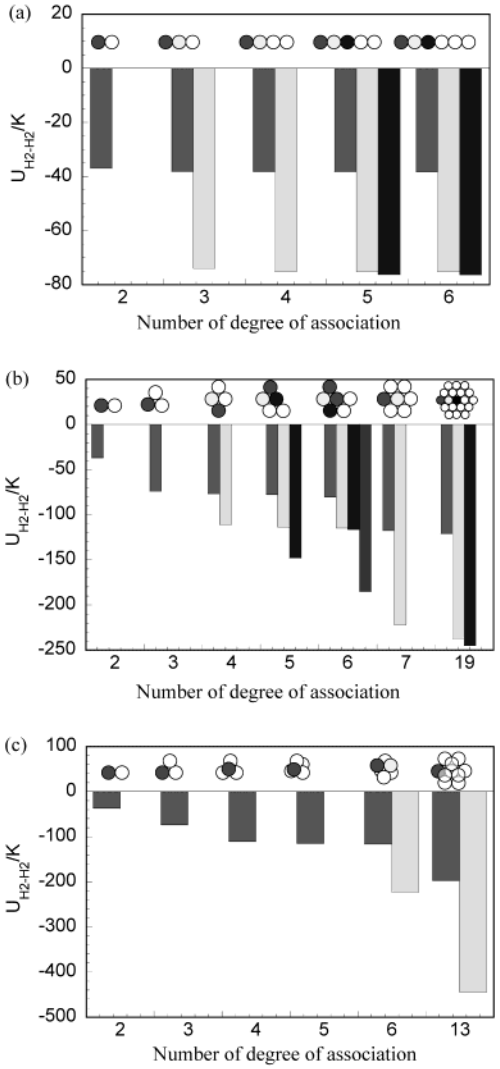

Figure 3. Fluid−fluid interaction U_{H2-H2} for a molecule occupying the different positions in the cluster of variable geometry and size: (a) 1-dimensional arrangement; (b) 2-dimensional arrangement; (c) 3-dimensional arrangement. U_{H2-H2} value for a molecule of an inherent color the same color.

adsorb hydrogen at an ambient temperature, hydrogen adsorption depends on the measuring temperature.

The contribution of interactions between hydrogen molecules U_{H2-H2} is important, because the Lennard-Jones parameter ϵ/k_B of a hydrogen molecule (37 K) is comparable to that of a hydrogen-graphene wall (32 K). Accordingly, the adsorbed hydrogen molecules can stabilize each other by the fluid−fluid interaction. For hydrogen adsorption, the contribution of the fluid−fluid interaction U_{H2-H2} is not small in comparison with the fluid−pore interaction. Figure 3 shows the fluid−fluid interaction potential depth that was calculated by the Lennard-Jones potential. Here the Lennard-Jones parameters of $\sigma_{ff} = 0.305$ nm and $\epsilon_{ff}/k_B = 37$ K were used for a hydrogen molecule. Also the intermolecular distance between the nearest neighbor molecules was presumed to be $2^{1/6}\sigma_{ff}$, which is the minimum position of the pair potential. Figure 3a shows U_{H2-H2} of the hydrogen molecules in the one-dimensional arrangement, which corresponds to those in the interstitial space. U_{H2-H2} at the end of the array is −40 K, and that at other locations is about −80 K. Thus, U_{H2-H2} is not large compared with the fluid−pore interaction.

Figure 3b shows the position dependence of U_{H2-H2} in the two-dimensional cluster of different size. This arrangement approximates hydrogen molecules in the submonolayer on the internal surface. The U_{H2-H2} value changes drastically with the cluster size and the location of a molecule. The larger the cluster size, the deeper the potential minimum. This is because the interaction potential minimum depends on the number of the pair interaction. U_{H2-H2} at the central position of the cluster is the deepest owing to the greatest pair number. The U_{H2-H2} values at the edge and center of the cluster consisting of 19 molecules are −120 and −240 K, respectively. These values are not small compared with the minimum of the fluid−pore interaction (−600 K at the monolayer adsorption position on the internal surface).

Figure 3c shows U_{H2-H2} of a molecule in the three-dimensional cluster. This cluster can be produced in the internal space of SWNHs. The U_{H2-H2} value at the edge position varies from −40 to −200 K and that at the central position of the 13-member cluster is −450 K. Thus, the maximum U_{H2-H2} in the three-dimensional cluster is about a half of the fluid−pore interaction potential. Consequently, the three-dimensional cluster can contribute to the stabilization of the adsorbed hydrogen in the internal space. This stabilization may be named *self-stabilization effect*. If this self-stabilization effect can be used more effectively, a larger amount of adsorbed hydrogen should be realized.

Hydrogen Adsorption Isotherms. Figure 4 shows the temperature dependence of hydrogen adsorption isotherms of SWNH and SWNH-ox. The adsorption equilibrium was achieved very quickly within 10 min and adsorption was reversible. Consequently, hydrogen is adsorbed by physical adsorption. According to our proposed classification, the adsorption isotherm of supercritical gas is classified into three types by the strength of the fluid−fluid interaction.[31] These are cooperative, virial, and Henry law types in the order of the interaction strength. The distinct difference between the three types of isotherms can be shown using the compression factor, Z_a, of the adsorbed layer vs the average adsorbed layer density, $\langle\rho_{ad}\rangle$, as follows.

$$Z_a = \frac{P}{\langle\rho_{ad}\rangle RT} \tag{3}$$

where P is the pressure of the bulk gas phase, R is the gas constant, and T is the temperature. The horizontal line, the linear increase, and the S-shaped increasing curve of $Z_a-\langle\rho_{ad}\rangle$ plots correspond to Henry, virial, and cooperative transition types, respectively. Both of adsorption isotherms of SWNH and SWNH-ox at 77 K are cooperative type, suggesting that adsorption sites are effective at 77 K. The saturated hydrogen adsorption of SWNH-ox at 77 K is 25 mg g^{-1}, and that of SWNH is 7 mg g^{-1}. Thus, SWNH-ox is more effective for hydrogen adsorption at 77 K than SWNH. The adsorption isotherm of SWNH-ox at 196 K is of virial type, indicating that adsorption sites are not so effective, whereas the adsorption isotherm of SWNH at 196 K belongs to the Henry type, showing a very weak interaction between hydrogen and SWNH. Thus SWNH interacts very weakly with hydrogen compared with SWNH-ox even at the same temperature, 196 K. Both of the adsorption isotherms at 303 K are of Henry type and thereby all of adsorption sites are too weak to adsorb hydrogen at 303 K. The adsorbed amounts of hydrogen on SWNH-ox and SWNH at 303 K and 6 MPa are 3 and 1 mg g^{-1}, respectively. As SWNH has only the interstitial pores and the internal SWNH space is completely closed, whereas SWNH-ox has both the interstitial pore and open internal SWNH space without a serious change of the assembly structure, adsorption processes of hydrogen in the interstitial pores and the internal spaces can be

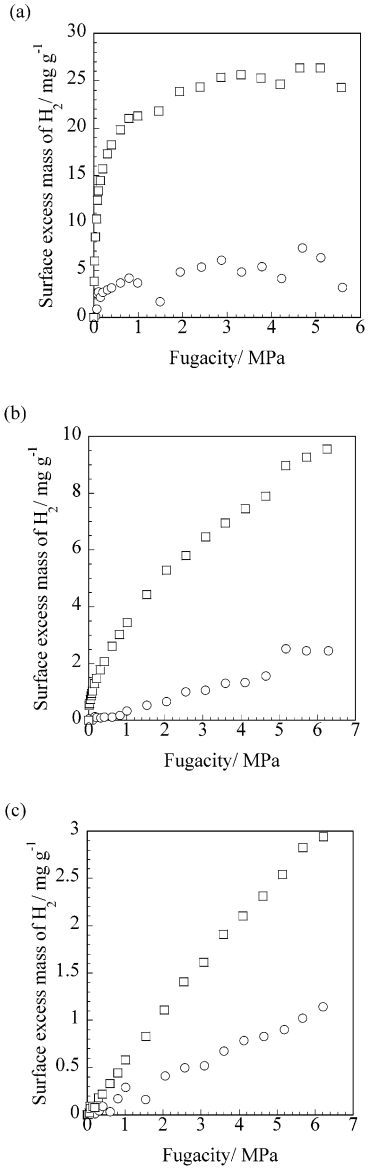

Figure 4. Adsorption isotherms of supercritical hydrogen on SWNH assemblies at different temperatures: (a) 77 K; (b) 196 K; (c) 303 K. Key: (○) SWNH; (□) SWNH-ox.

separated by subtraction of the adsorption isotherm of SWNH from that of SWNH-ox. Hence the average adsorbed densities of hydrogen in the interstitial (external) pores $\langle\rho_{ad}\rangle_{ext}$ and internal spaces $\langle\rho_{ad}\rangle_{in}$ are derived by eqs 4 and 5, respectively.

$$\langle\rho_{ad}\rangle_{ext} = \frac{n_{ex}(\text{SWNH})}{V_0(\text{SWNH})} + \rho_{bulk} \quad (4)$$

$$\langle\rho_{ad}\rangle_{in} = \frac{n_{ex}(\text{SWNH-ox}) - n_{ex}(\text{SWNH})}{V_0(\text{SWNH-ox}) - V_0(\text{SWNH})} + \rho_{bulk} \quad (5)$$

Here, V_0 is the pore volume (mL/g). Subscripts "ext" and "in" express the interstitial pore and the internal spaces, respectively.

Figure 5 shows the separated adsorption isotherms of hydrogen in internal spaces and interstitial (external) pores at different temperatures. The shapes of the adsorption isotherms at different temperatures in Figure 5 are close to those in Figure 4. The most important thing in Figure 5 is that $\langle\rho_{ad}\rangle_{in} > \langle\rho_{ad}\rangle_{ext}$ at 77 and 196 K, though the interaction potential minimum at the internal monolayer sites is much shallower than that at the

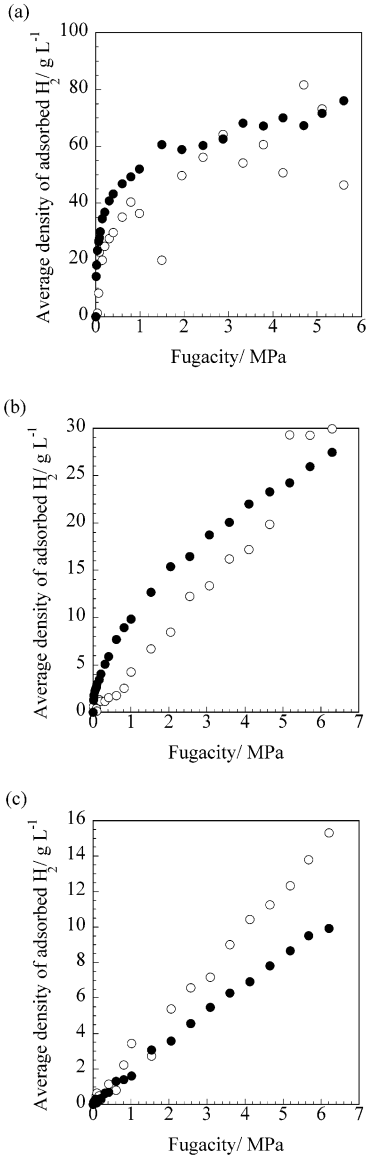

Figure 5. Adsorption isotherms of supercritical hydrogen in (●) internal and (○) external spaces of SWNH at different temperatures: (a) 77 K; (b) 196 K; (c) 303 K.

TABLE 2: Microporosity of Internal and Interstitial Spaces for SWNH Assembly

	specific sruface area, $m^2\ g^{-1}$	pore volume, mL g^{-1}
internal space	318	0.36
external pore (interstitial)	200	0.11

interstitial (external) sites. The separated porosity of SWNH-ox is shown in Table 2. The pore volume of the internal spaces is 0.36 mL g^{-1}, whereas the pore volume of the external pores is 0.11 mL g^{-1}. The pore volume of the internal spaces must be divided into the monolayer sites of the greater interaction potential and the central zone of the smaller interaction potential; the internal space from the monolayer area is nearly half of the pore volume.[19] Therefore, it is quite unusual that $\langle\rho_{ad}\rangle_{in} > \langle\rho_{ad}\rangle_{ext}$. From the simple consideration on the interaction potential and pore volume, $\langle\rho_{ad}\rangle_{in}$ must be smaller than $\langle\rho_{ad}\rangle_{ext}$. Hence, this fact strongly indicates the presence of the special enhancement effect of adsorption.

Cole et al. suggested that preadsorbed molecules in the interstitial sites can stabilize a molecule in an internal space of the SWNT in the case of the SWNT parallel arrays in their

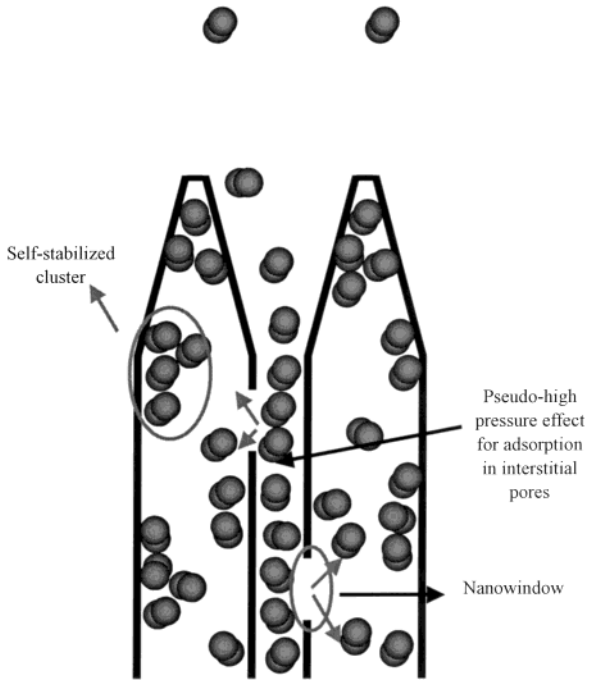

Figure 6. Self-locking adsorption mechanism.

theoretical study.[32] However, the contribution of this effect is only −1.2 K for this system. On the other hand, Ohba and Kaneko showed that the preformed monolayer stabilizes significantly the second layer adsorption in N_2 adsorption in the slit-shaped carbon micropores at 77 K.[33] In a similar way, preadsorbed hydrogen assemblies should stabilize the subsequent hydrogen adsorption, which is designated as a self-stabilization effect. The minimum contributions by the fluid−fluid interaction in the interstitial pore and internal space are −75 and −450 K (see Figure 3a,c), respectively. The additional stabilization of the hydrogen adsorbed on the monolayer sites, which was discussed above, should be noted for the adsorption enhancement. However, it cannot explain the observed fact of $\langle\rho_{ad}\rangle_{in} > \langle\rho_{ad}\rangle_{ext}$, because the depth of total interaction potential U_{to} of the interstitial pore is deeper than that of the internal space by 100 K, where $U_{to} = U_{sf} + U_{H2-H2}$. Thus another enhancement mechanism is necessary. Moreover, the enhancement mechanism must interpret the conversion of the relative adsorption amount at 303 K.

In this case, molecules are adsorbed in the interstitial pores at first. Therefore adsorption of molecules in internal pores through the nanowindows begins under a pressure much high than that of the bulk gas phase, inducing the observed enhancement in adsorption in the internal pores. This enhancement mechanism is named a self-locking adsorption mechanism. This is because adsorbed molecules around nanowindows in the interstitial pores can behave as if they block desorption from the internal pores. This situation is illustrated in Figure 6.

Temperature Dependence of Interaction. Virial analysis provides information on the interaction is associated with the above model. The virial equation for an adsorbed layer is expressed by[34,35]

$$\ln\left(\frac{\rho_{ad}}{F}\right) = \ln(k_H) + B_2\rho_{ad} \qquad (6)$$

where k_H is the Henry law constant, which is the scale of the fluid−wall interaction, and B_2 is the second virial coefficient, which expresses the fluid−fluid interaction. The virial plots are

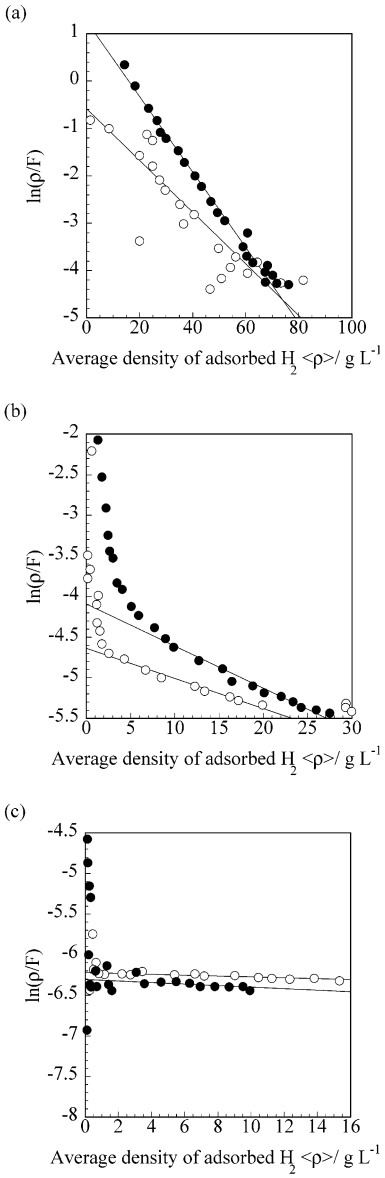

Figure 7. Virial plots of supercritical hydrogen adsorption isotherm: (●) internal and (○) interstitial spaces of SWNH. Temperature: (a) 77 K; (b) 196 K; (c) 303 K.

shown in Figure 7. k_H and B_2 are obtained by the linear region of the virial plots. The virial plot varies with the measuring temperature distinctly. Good linear plots are obtained at 77 K and the plot of SWNH-ox has a larger slope than that of SWNH at 77 K; the k_H of SWNH-ox is greater than that of SWNH. Although the virial plots at 196 K do not provide a simple linear relation, there is a linear region. Also the k_H of SWNH-ox, which is much smaller than that at 77 K, is larger than that of SWNH. The virial plots at 303 K give an almost horizontal line, whose slopes are quite small compared with others. Figure 8 shows the van't Hoff plot of k_H and the temperature dependence of B_2. As to the B_2−temperature relation, that of the bulk gas is shown for comparison. Although the van't Hoff plots are slightly convex, suggesting the presence of a repulsive interaction hydrogen adsorption at low temperature, we applied the van't Hoff relation. Their slopes lead to the enthalpy difference at the zero coverage $\Delta H_{ad,0}$ between adsorbed and gaseous states;[34] the obtained $\Delta H_{ad,0}$ values for the internal space and interstitial pore are 3 and 2 kJ mol^{-1}, respectively. Although the interstitial pores give a deeper potential well than the internal spaces, both $\Delta H_{ad,0}$ values are almost similar, taking into account the error

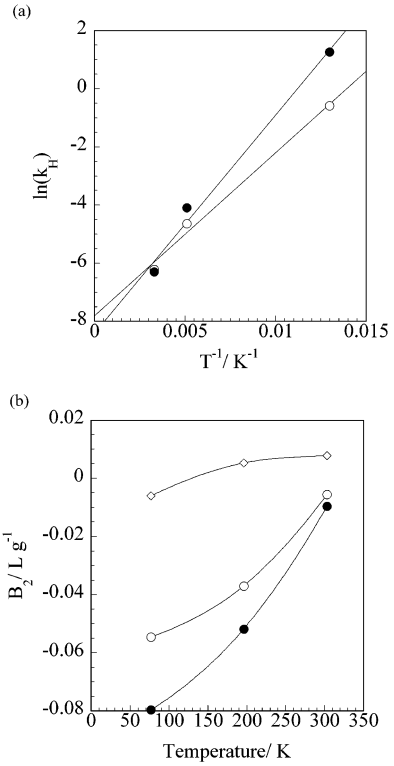

Figure 8. Temperature dependence of the (a) Henry law constant and (b) second virial coefficient for hydrogen adsorption: (●) internal and (○) interstitial spaces of SWNH; (◇) bulk gas phase.

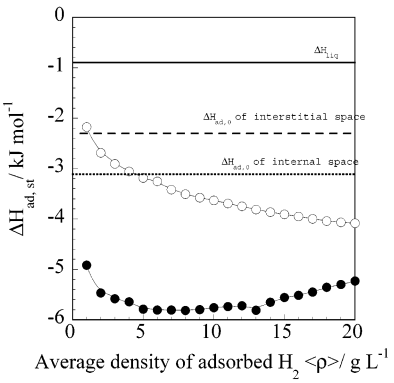

Figure 9. Differential isosteric enthalpy changes of physical adsorption of hydrogen on SWNHs: (●) internal and (○) interstitial spaces of SWNH.

of the virial plot for the hydrogen adsorption. The average kinetic energy must be several kelvins and thereby these $\Delta H_{ad,0}$ values are reasonable. However, we cannot use this $\Delta H_{ad,0}$ value for a detailed discussion.

The greater B_2 value in the negative direction suggests a stronger fluid−fluid interaction. The fluid−fluid interactions in the pores of SWNH are much more intense than that of bulk gas. In particular, the fluid−fluid interaction in the internal pores is greater than that in the external pores at 77 and 196 K. The B_2−temperature relation also supports the above mechanism, showing that the contribution of the fluid−fluid interaction is more significant at low temperature.

Excess Stabilization Enthalpy and Adsorption Mechanism. The differential isosteric enthalpy change of adsorption $\Delta H_{ad,st}$ was determined from the adsorption isotherms in the interstitial and internal spaces at different temperatures (Figure 5) using the Clapeyron−Clausius equation. The $\Delta H_{ad,st}$ values vs the average adsorbed density are shown in Figure 9. The adsorbed

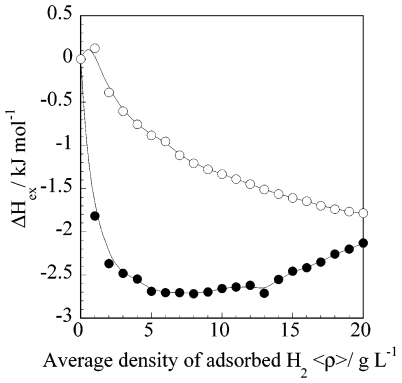

Figure 10. Self-stabilization enthalpy change with the average adsorbed density: (●) internal and (○) interstitial spaces of SWNH.

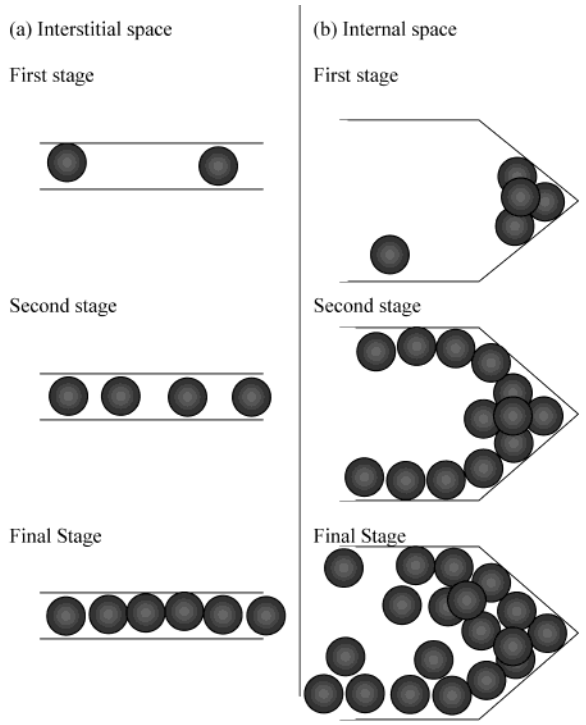

Figure 11. Hydrogen adsorption processes in (a) interstitial and (b) internal spaces of SWNH assembly.

hydrogen molecules at the interstitial and internal spaces are stabilized by more than −1 and −4 kJ mol^{-1}, respectively, from the enthalpy of liquefaction (−0.898 kJ mol^{-1}).[36] The $\Delta H_{ad,st}$ for the interstitial space decreases with the average adsorbed density, whereas that for the internal space is nearly constant. The difference, ΔH_{ex}, between $\Delta H_{ad,st}$ and $\Delta H_{ad,0}$ provides the scale of the self-stabilization effect due to the cluster formation, which was discussed above.

The relationship between ΔH_{ex} and the average adsorbed density is shown in Figure 10. The ΔH_{ex} of interstitial space is higher than that of internal space. Hence, the excess stabilization in the internal space is stronger than that in the interstitial space, because the sign of ΔH_{ex} is negative. This fact coincides with the above-mentioned interaction potential results. The ΔH_{ex} gradually decreases with the increase of $\langle\rho\rangle$ for the interstitial space. This suggests that the cluster growth proceeds gradually with the increase of $\langle\rho\rangle$, as illustrated in Figure 11a. On the other hand, the ΔH_{ex} in the internal space drops in the low $\langle\rho\rangle$ region, keeping an almost constant value after the initial drop. Because there is a cone site having a strong interaction potential in the internal space, hydrogen molecules should be adsorbed

in the cone site to form the three-dimensional cluster even at the low $\langle\rho\rangle$ region, giving the adsorption drop. Then, the cluster grows along the internal tube wall. Figure 11b shows the above-mentioned adsorption process; the cluster is formed in the cone site at first and then it extends along the internal pore wall, according with the cluster grown in the radial direction. Thus, the ΔH_{ex} data give the adsorption mechanism of hydrogen in SWNH assemblies.

Conclusion

Adsorption isotherms of hydrogen in internal and interstitial spaces of SWNH assemblies were determined experimentally, providing the adsorbed density of hydrogen in internal and interstitial spaces. The fact that the adsorbed density of hydrogen in interstitial spaces is lower than that in internal spaces against the prediction from the interaction potential calculation was explained by the self-stabilization effect of the self-locking mechanism. Here, the self-stabilization effect and self-locking mechanism come from the cluster formation by hydrogen molecules and the presence of strongly adsorbed molecules in the interstitial spaces, respectively.

Acknowledgment. This work was funded by Grant-in-Aid for Scientific Research B and the Grant for Advanced Science from the Japanese Government. D.K. and S.I. acknowledge the support by the U.S. Office of Naval Research (ONR-N000140010762).

References and Notes

(1) Chambers, A.; Park, C.; Baker, R. T. K.; Roddriguez, N. M. *J. Phys. Chem. B* **1998**, *102*, 4253.

(2) Dillon, A. C.; Jones, K. M.; Bekkedahl, T. A.; Kiang, C. H.; Bethune, D. S.; Heben, M. J. *Nature* **1997**, *386*, 377.

(3) Iijima, S.; Ichihashi, T. *Nature* **1993**, *363*, 603.

(4) Chen, P.; Wu, X.; Lin, J.; Tan, K. L. *Science* **1999**, *285*, 91.

(5) Zandonella, C. *Nature* **2001**, *410*, 734.

(6) Murata, K.; Hanzawa, Y.; Kaneko, K. *Adv. Eng. Mater*., in press.

(7) Wang, Q.; Johnson, J. K. *J. Chem. Phys.* **1999**, *110*, 577.

(8) Wang, Q.; Johnson, J. K. *J. Phys. Chem. B* **1999**, *103*, 277.

(9) Lee, S. M.; Lee, Y. H. *Appl. Phys. Lett*. **2000**, *76*, 2877.

(10) Dresselhaus, M. S.; Williams, K. A.; Eklund, P. C. *MRS Bull.* **1999**, *24*, 45.

(11) Iijima, S.; Yudasaka, M.; Yamada, R.; Bandow, S.; Suenaga, K.; Kokai, F.; Takahashi, K. *Chem. Phys. Lett.* **1999**, *309*, 165.

(12) Bekyarova, E.; Hanzawa, Y.; Kaneko, K.; Silvestre-Albero, J.; Sepulveda-Escribano, A.; Rodriguez-Reinoso, F.; Kasuya, D.; Yudasaka, M.; Iijima, S. *Chem. Phys. Lett.*, in press.

(13) Kaneko, K.; Ishii, C. *Colloid Surf.* **1992**, *67*, 203.

(14) Setoyama, N.; Suzuki, T.; Kaneko, K. *Carbon* **1998**, *36*, 1459.

(15) The particle density is defined as $\rho_p = 1/(V_s + V_c)$, where V_s is the solid part volume of the sample and ρ_c is the volume of pores in which He is not accessible.

(16) Murata, K.; Kaneko, K.; Kokai, F.; Takahashi, K.; Yudasaka, M.; Iijima, S. *Chem. Phys. Lett.* **2000**, *331*, 14.

(17) Kaneko, K.; Shimizu, K.; Suzuki, T. *J. Chem. Phys.* **1992**, *97*, 8705.

(18) Murata, K.; Kaneko, K.; Steele, W. A.; Kokai, F.; Takahashi, K.; Kasuya, D.; Yudasaka, M.; Iijima, S. *Nano Lett.* **2001**, *1*, 197.

(19) Murata, K.; Kaneko, K.; Steele, W. A.; Kokai, F.; Takahashi, K.; Kasuya, Hirahara, K.; Yudasaka, M.; Iijima, S. *J. Phys. Chem. B* **2001**, *105*, 10210.

(20) Murata, K.; Miyawaki, J.; Kaneko, K. *Carbon* **2002**, *40*, 425.

(21) Gibbs, J. W. *Collected Works*; Longmans Green and Co.: New York, 1877.

(22) Yang, D. M.; Crowell, A. D. *Physical Adsorption of Gases*; Butterworth: Washington, DC, 1962.

(23) Murata, K.; Kaneko, K. *Chem. Phys. Lett.* **2000**, *321*, 342.

(24) Murata, K.; El-Merraoui, M.; Kaneko, K. *J. Chem. Phys*. **2001**, *114*, 4196.

(25) Sircar, S. *Ind. Eng. Chem. Res*. **1999**, *38*, 3670.

(26) Salem, M. M. K.; Braeuer, P.; Szombathely, M. v.; Heuchel, M.; Harting, P.; Quitzsch, K.; Jaroniec, M. *Langmuir* **1998**, *14*, 3376.

(27) Miyawaki, J.; Kaneko, K. *Chem. Phys. Lett.* **2001**, *337*, 243.

(28) Murata, K.; Miyawaki, J.; Kaneko, K. *Fundamental of Adsorption 7*; IK International: Chiba, 2002; p 664.

(29) Steele, W. A.; Bojan, M. J. *Adv. Colloid Interface Sci*. **1998**, *77*−*76*, 153.

(30) Bandow, S.; Kokai, F.; Takahashi, K.; Yudasaka, M.; Qin, L. C.; Iijima, S. *Chem. Phys. Lett*. **2000**, *321*, 514.

(31) Murata, K.; Yudasaka, M.; Iijima, S.; El-Merraoui, M.; Kaneko, K. *J. Appl. Phys.* **2002**, *91*, 10227.

(32) Cole, M. W.; Crespi, V. H.; Stan, G.; Ebner, C.; Hartman, J. M.; Moroni, S.; Boninsegni, M. *Phys. Rev. Lett*. **2000**, *84*, 3883.

(33) Ohba, T.; Suzuki, T.; Kaneko, K. *Chem. Phys. Lett*. **2000**, *326*, 158.

(34) Ross, S.; Olivier, J. P. *On Physical Adsorption*; Interscience: New York, 1964.

(35) Zhang, S.-Y.; Talu, O.; Hayhurst, D. T. *J. Phys. Chem.* **1991**, *95*, 1722.

(36) *CRC Handbook of Chemistry and Physics*, 76th ed.; Lide, D. R., Ed.; CRC Press: New York, 1995.